Available online at www.sciencedirect.com

ScienceDirect

Nuclear Physics B 900 (2015) 273–294

NUCLEAR PHYSICS B

www.elsevier.com/locate/nuclphysb

Double-quarkonium production at a fixed-target experiment at the LHC (AFTER@LHC)

Jean-Philippe Lansberg [a], Hua-Sheng Shao [b,*]

[a] *IPNO, Université Paris-Sud, CNRS/IN2P3, F-91406, Orsay, France*
[b] *PH Department, TH Unit, CERN, CH-1211, Geneva 23, Switzerland*

Received 28 April 2015; received in revised form 14 August 2015; accepted 14 September 2015

Available online 24 September 2015

Editor: Hong-Jian He

Abstract

We present predictions for double-quarkonium production in the kinematical region relevant for the proposed fixed-target experiment using the LHC beams (dubbed as AFTER@LHC). These include all spin-triplet S-wave charmonium and bottomonium pairs, *i.e.* $\psi(n_1S)+\psi(n_2S)$, $\psi(n_1S)+\Upsilon(m_1S)$ and $\Upsilon(m_1S)+\Upsilon(m_2S)$ with $n_1,n_2=1,2$ and $m_1,m_2=1,2,3$. We calculate the contributions from double-parton scatterings and single-parton scatterings. With an integrated luminosity of 20 fb^{-1} to be collected at AFTER@LHC, we find that the yields for double-charmonium production are large enough for differential distribution measurements. We discuss some differential distributions for $J/\psi+J/\psi$ production, which can help to study the physics of double-parton and single-parton scatterings in a new energy range and which might also be sensitive to double intrinsic $c\bar{c}$ coalescence at large negative Feynman x.

1. Introduction

Heavy-quarkonium production is typically a multi-scale process, which involves both short- and long-distance facets of the strong interaction. This particularity makes heavy-quarkonium production an ideal probe to study Quantum Chromodynamics (QCD) in its perturbative and non-perturbative regimes simultaneously. Studies have extensively been performed at collider

* Corresponding author.
E-mail address: huasheng.shao@cern.ch (H.-S. Shao).

http://dx.doi.org/10.1016/j.nuclphysb.2015.09.005

and fixed-target energies in proton–proton, proton–nucleus and nucleus–nucleus collisions (see reviews *e.g.* Refs. [1–3]). The associated production of heavy quarkonium is a very interesting process not only because it provides a way to pin down the heavy-quarkonium production mechanism but also because it can help to understand a new dynamics of hadron collisions appearing at high energies, where multiple scatterings of partons (MPS) happen simultaneously, among which the most likely are of course two short-distance interactions from a single hadron–hadron collision – double-parton scattering (DPS). A number of experimental studies relevant for DPS analyses with heavy quarkonia have recently been carried out such as $J/\psi + W$ [4], $J/\psi + Z$ [5], J/ψ + charm [6] and $J/\psi + J/\psi$ [7] production.

In particular, the latter process, *i.e.* double-quarkonium production, is of specific interest. It provides an original tool to study the quarkonium production from the conventional single-parton scatterings (SPSs), whose contribution has theoretically been studied in many works [8–19]. Moreover, it has been claimed in Refs. [20–25,18,19] that DPS contributions should be a significant source of $J/\psi + J/\psi$, especially at high energies where there is a high gluon flux. On the experimental side, the spin-triplet S-waves (*e.g.* J/ψ, ψ', $\Upsilon(nS)$) provide clean signatures with their small background when they are studied in their decay into muon pairs. They are easy to trigger on, in contrast to hadronic jets and open-charm meson productions, which require either good calorimetry or good particle identification.

A first comprehensive comparison between experiments [26,7,27] and theory for J/ψ-pair production at the Tevatron and the LHC has been performed in Ref. [18], where we have pointed out that this observable could be used to probe different mechanisms in different kinematical regions. We noted that the direct DPS measurement by D0 Collaboration [7] – looking at the rapidity-difference spectrum – is consistent with the J/ψ-pair measurement by the CMS Collaboration [27] and, as we will discuss later on, compatible with rather large DPS rates. On the other hand, as we advocated in [16], one cannot draw a definite conclusion on the presence of DPS in the early LHCb data [26] with their relatively low statistics.

In this context, we find it important to study the potentialities offered by the use of the 7 TeV proton LHC beams in the fixed-target mode to study quarkonium-pair production. Its multi-TeV beams indeed allow one to study $p + p$, $p + d$ and $p + A$ collisions at a centre-of-mass energy $\sqrt{s_{NN}} \simeq 115$ GeV as well as Pb $+ p$ and Pb $+ A$ collisions at $\sqrt{s_{NN}} \simeq 72$ GeV, with the high precision typical of the fixed-target mode. It has indeed been advocated in [28,29] that such a facility, referred to as AFTER@LHC, would become a quarkonium, prompt photon and heavy-flavour observatory thanks to its large expected luminosity (for recent phenomenological studies, see [30–39]). A first feasibility study for quarkonium production was presented in [40] and demonstrated that a LHCb-like detector would perform extremely well in the fixed-target mode. Similar performances are expected for quarkonium-pair production.

Integrated luminosities as large as 20 fb^{-1} [28] can be delivered during a one-year run of p + H collisions with a bent crystal to extract the beam [41]. The LHC beam can also go through an internal-gas-target system.[1] Conservatively sticking to gas pressures already reachable now, yearly integrated luminosities reach 100 pb^{-1}. With a designed target cell similar to that of HERMES [45], a few fb^{-1} yr^{-1} are probably also easily reachable [46]. We have reported in Table 1 the instantaneous and yearly integrated luminosities expected with the proton beams on various target species of various thicknesses, for both options.

[1] This is in fact already tested at low gas pressures by the LHCb Collaboration in order to monitor the luminosity of the beam [42–44].

Table 1
Expected luminosities obtained for a 7 TeV proton beam extracted by means of a bent crystal or obtained with an internal gas target with a pressure similar to that of SMOG@LHCb [43].

Beam	Target	Thickness (cm)	ρ (g cm^{-3})	$\mathcal{L}$ (μb^{-1} s^{-1})	$\int \mathcal{L}$ (pb^{-1} y^{-1})
p	Liquid H	100	0.068	2000	20 000

Beam	Target	Usable gas zone (cm)	Pressure (Bar)	$\mathcal{L}$ (μb^{-1} s^{-1})	$\int \mathcal{L}$ (pb^{-1} y^{-1})
p	Perfect gas	100	10^{-9}	10	100

The structure of this paper is as follows. In Section 2, we detail and justify our methodology to compute both DPS and SPS contributions to quarkonium-pair production. Section 3 contains a general discussion of the interest to look at DPS vs SPS contributions at different energies. Section 4 presents a comparison between results up to α_s^4 and α_s^5. This prepares the discussion of our results at $\sqrt{s} = 115$ GeV relevant for AFTER@LHC in Section 5. Section 6 gathers our conclusions.

2. Methodology

In this section, we explain the main ingredients used to compute the rates for double-quarkonium production at AFTER@LHC, which closely follows from our previous work in Ref. [18].

2.1. Double-parton scatterings

The description of such a mechanism is usually done by assuming that DPSs can be factorised into two single-parton scatterings (SPS) resulting each in the production of a quarkonium. This can be seen as a first rough approximation which can however be justified by the fact that possible unfactorisable corrections due to parton correlations could be small at small x. In the case of the double-quarkonium production, the master formula from which one starts under the factorisation assumption is (see *e.g.* Ref. [24])

$$\sigma_{\mathcal{Q}_1\mathcal{Q}_2} = \frac{1}{1+\delta_{\mathcal{Q}_1\mathcal{Q}_2}} \sum_{i,j,k,l} \int dx_1 dx_2 dx_1' dx_2' d^2\mathbf{b}_1 d^2\mathbf{b}_2 d^2\mathbf{b} \times \Gamma_{ij}(x_1, x_2, \mathbf{b}_1, \mathbf{b}_2)\, \hat{\sigma}_{ik}^{\mathcal{Q}_1}(x_1, x_1')\, \hat{\sigma}_{jl}^{\mathcal{Q}_2}(x_2, x_2')\, \Gamma_{kl}(x_1', x_2', \mathbf{b}_1 - \mathbf{b}, \mathbf{b}_2 - \mathbf{b}), \quad (1)$$

where $\Gamma_{ij}(x_1, x_2, \mathbf{b}_1, \mathbf{b}_2)$ is the generalised double distributions with the longitudinal fractions x_1,x_2 and the transverse impact parameters $\mathbf{b}_1$ and $\mathbf{b}_2$, $\hat{\sigma}_{jk}^{\mathcal{Q}_i}(x_l, x_l')$ are the usual partonic cross sections for single quarkonium production and $\delta_{\mathcal{Q}_1\mathcal{Q}_2}$ is the Kronecker delta function. A further factorisation assumption is to decompose $\Gamma_{ij}(x_1, x_2, \mathbf{b}_1, \mathbf{b}_2)$ into a longitudinal part and a transverse part

$$\Gamma_{ij}(x_1, x_2, \mathbf{b}_1, \mathbf{b}_2) = D_{ij}(x_1, x_2) T_{ij}(\mathbf{b}_1, \mathbf{b}_2), \quad (2)$$

where $D_{ij}(x_1, x_2)$ is the double-parton distribution functions (dPDF) [47]. Moreover, by ignoring the correlations between partons produced from each hadrons, one can further assume

$$D_{ij}(x_1, x_2) = f_i(x_1) f_j(x_2),$$
$$T_{ij}(\mathbf{b}_1, \mathbf{b}_2) = T_i(\mathbf{b}_1) T_j(\mathbf{b}_2), \tag{3}$$

where $f_i(x_1)$ and $f_j(x_2)$ are the normal single PDFs. This yields to

$$\sigma_{\mathcal{Q}_1\mathcal{Q}_2} = \frac{1}{1+\delta_{\mathcal{Q}_1\mathcal{Q}_2}} \sum_{i,j,k,l} \sigma_{ik\to\mathcal{Q}_1}\sigma_{jl\to\mathcal{Q}_2} \int d^2\mathbf{b} \int T_i(\mathbf{b}_1) T_k(\mathbf{b}_1 - \mathbf{b}) d^2\mathbf{b}_1 \times \int T_j(\mathbf{b}_2) T_l(\mathbf{b}_2 - \mathbf{b}) d^2\mathbf{b}_2. \tag{4}$$

If one also ignores the parton flavour dependence in $T_{i,j,k,l}(\mathbf{b})$ and defines the overlapping function

$$F(\mathbf{b}) = \int T(\mathbf{b}_i) T(\mathbf{b}_i - \mathbf{b}) d^2\mathbf{b}_i, \tag{5}$$

one reaches the so-called "pocket formula"

$$\sigma_{\mathcal{Q}_1\mathcal{Q}_2} = \frac{1}{1+\delta_{\mathcal{Q}_1\mathcal{Q}_2}} \frac{\sigma_{\mathcal{Q}_1}\sigma_{\mathcal{Q}_2}}{\sigma_{\text{eff}}}, \tag{6}$$

where $\sigma_{\mathcal{Q}_1}$ and $\sigma_{\mathcal{Q}_2}$ are the cross sections for respectively single $\mathcal{Q}_1$ and $\mathcal{Q}_2$ production and σ_{eff} is a parameter to characterise an effective spatial area of the parton–parton interactions via

$$\sigma_{\text{eff}} = \left[\int d^2\mathbf{b} F(\mathbf{b})^2 \right]^{-1}. \tag{7}$$

Under these assumptions, it is only related to the initial state and should be independent of the final state. However, the validation of its universality (process independence as well as energy independence) and the factorisation in Eq. (6) should be cross checked case by case. In a fact, some factorisation-breaking effects have recently been identified (see *e.g.* [48–50]). Thanks to its larger luminosity and its probably wide rapidity coverage, AFTER@LHC provides a unique opportunity to probe DPS and to extract σ_{eff} from double-quarkonium final states.

To perform our predictions, we will use $\sigma_{\text{eff}} = 5.0 \pm 2.75$ mb, which was determined from J/ψ-pair production data at the Tevatron by D0 Collaboration [7].[2] The reason for such a choice is that all of the double-quarkonium-production processes share the same gluon–gluon initial states and the typical x are not that much different. This also means that we only need to assume the energy independent of σ_{eff}. However, we do not claim that this value is the only one possible; we only take it as our reference number. If one wants to use another value of σ_{eff}, one can just simply perform a rescaling (proportional to $1/\sigma_{\text{eff}}$) of the numbers given in the following.

Since the description of single heavy-quarkonium production at hadron colliders in the whole kinematical region is still a challenge to theorists, using *ab initio* theoretical computation of $\sigma_{\mathcal{Q}}$ would significantly inflate theoretical uncertainties. Instead, we will work in a data-driven way to determine $\sigma_{\mathcal{Q}}$.

Our procedure is as follows. We start from the cross section $\sigma_{\mathcal{Q}_i}$ which can be written as

$$\sigma(pp \to \mathcal{Q} + X) = \sum_{a,b} \int dx_1 dx_2 f_a(x_1) f_b(x_2) \frac{1}{2\hat{s}} \overline{|\mathcal{A}_{ab\to\mathcal{Q}+X}|^2} d\text{LIPS}_{\mathcal{Q}+X}, \tag{8}$$

[2] Note that Ref. [7] has updated the value of σ_{eff} to be 4.8 ± 2.55 mb. However, since the difference is very small, we still used the original one.

Table 2
Results of a fit of $d^2\sigma/dP_T dy$ to (a) the $\psi(nS)$ PHENIX data [51] by fixing $n = 2$ and $\langle P_T\rangle = 4.5$ GeV and (b) the $\Upsilon(nS)$ data CDF [52] data by fixing $n = 2$ and $\langle P_T\rangle = 13.5$ GeV. Only the $> 1\%$ errors are given.

	κ	λ	# of data	χ^2
J/ψ	0.67 ± 0.08	0.38	51	422
$\psi(2S)$	0.15 ± 0.03	0.35	4	1.12

(a) Charmonia

	κ	λ	# of data	χ^2
$\Upsilon(1S)$	0.89	0.084 ± 0.0061	14	29
$\Upsilon(2S)$	0.79	0.056	9	2.2
$\Upsilon(3S)$	0.68 ± 0.029	0.046	9	3.9

(b) Bottomonia

where f_a, f_b are the parton distribution functions (PDF) of the initial partons a and b, $d\text{LIPS}_{\mathcal{Q}+X}$ is the Lorentz-invariant phase-space measure for $pp \to \mathcal{Q} + X$ and $\sqrt{\hat{s}}$ is the partonic centre-of-mass energy (*i.e.* $\hat{s} = x_1 x_2 s$). For single quarkonium production in $p + p$ collisions at $\sqrt{s} = 115$ GeV, the gluon–gluon initial state is dominant. The initial colour and helicity averaged amplitude square for $gg \to \mathcal{Q} + X$ can be expressed in the form of a crystal ball function [20]

$$\overline{|\mathcal{A}_{gg\to\mathcal{Q}+X}|^2} = \begin{cases} K \exp(-\kappa \frac{P_T^2}{M_{\mathcal{Q}}^2}) & \text{when } P_T \le \langle P_T\rangle \\ K \exp(-\kappa \frac{\langle P_T\rangle^2}{M_{\mathcal{Q}}^2}) \left(1 + \frac{\kappa}{n} \frac{P_T^2 - \langle P_T\rangle^2}{M_{\mathcal{Q}}^2}\right)^{-n} & \text{when } P_T > \langle P_T\rangle \end{cases} \tag{9}$$

where $K = \lambda^2 \kappa \hat{s}/M_{\mathcal{Q}}^2$. The parameters κ, λ, n and $\langle P_T\rangle$ can be determined by fitting the (differential) cross sections to the experimental data. The dedicated codes to perform the fit and to compute the DPS contributions to double-quarkonium production have been implemented in HELAC-ONIA [53,54].

Once a fit is done, $|\mathcal{A}_{gg\to\mathcal{Q}+X}|^2$ is fixed and it allows us to evaluate $\sigma(pp \to \mathcal{Q} + X)$ (or its differential counterparts in any variable) which can then be injected into the "pocket formula" Eq. (6) in order to predict the DPS yield. Since we do not apply any muon cuts, we do not need to make any assumptions regarding the polarisation of the production quarkonia.

The code was tested and, with the same parameters as in Ref. [20], we have reproduced their results. However, their combined fit of the charmonium data taken at the Tevatron and the LHC cannot reproduce well the low-energy data measured by PHENIX Collaboration [51] at RHIC. Since the collision energy of RHIC $\sqrt{s} = 200$ GeV is very close to the centre-of-mass energy of the fixed-target experiment at the LHC (AFTER@LHC), *i.e.* $\sqrt{s} = 115$ GeV, we prefer to use the PHENIX data alone to determine the parameters in Eq. (9). A fit of $d^2\sigma/dP_T dy$ to the PHENIX data [51] for J/ψ and $\psi(2S)$ production gives the χ^2 results presented in Table 2a having fixed $n = 2$ and $\langle P_T\rangle = 4.5$ GeV. We also show the comparisons of the P_T spectra in Fig. 1a–c. The large χ^2 for the single J/ψ production can be reduced to 55.8 when one only considers the 23 PHENIX data points in the central region (*i.e.* $|y_{J/\psi}| < 0.35$) and excluding the lowest-P_T bin. A fit to the sole PHENIX data in the forward region $1.2 < |y_{J/\psi}| < 2.4$ changes κ by $\sim 15\%$ and λ by $\sim 5\%$. However, the main uncertainty in predicting DPS contributions to double ψ production remains from that of σ_{eff} and those from these fits are in practice nearly irrelevant for our predictions. This is obvious for λ which only affects the normalisation.

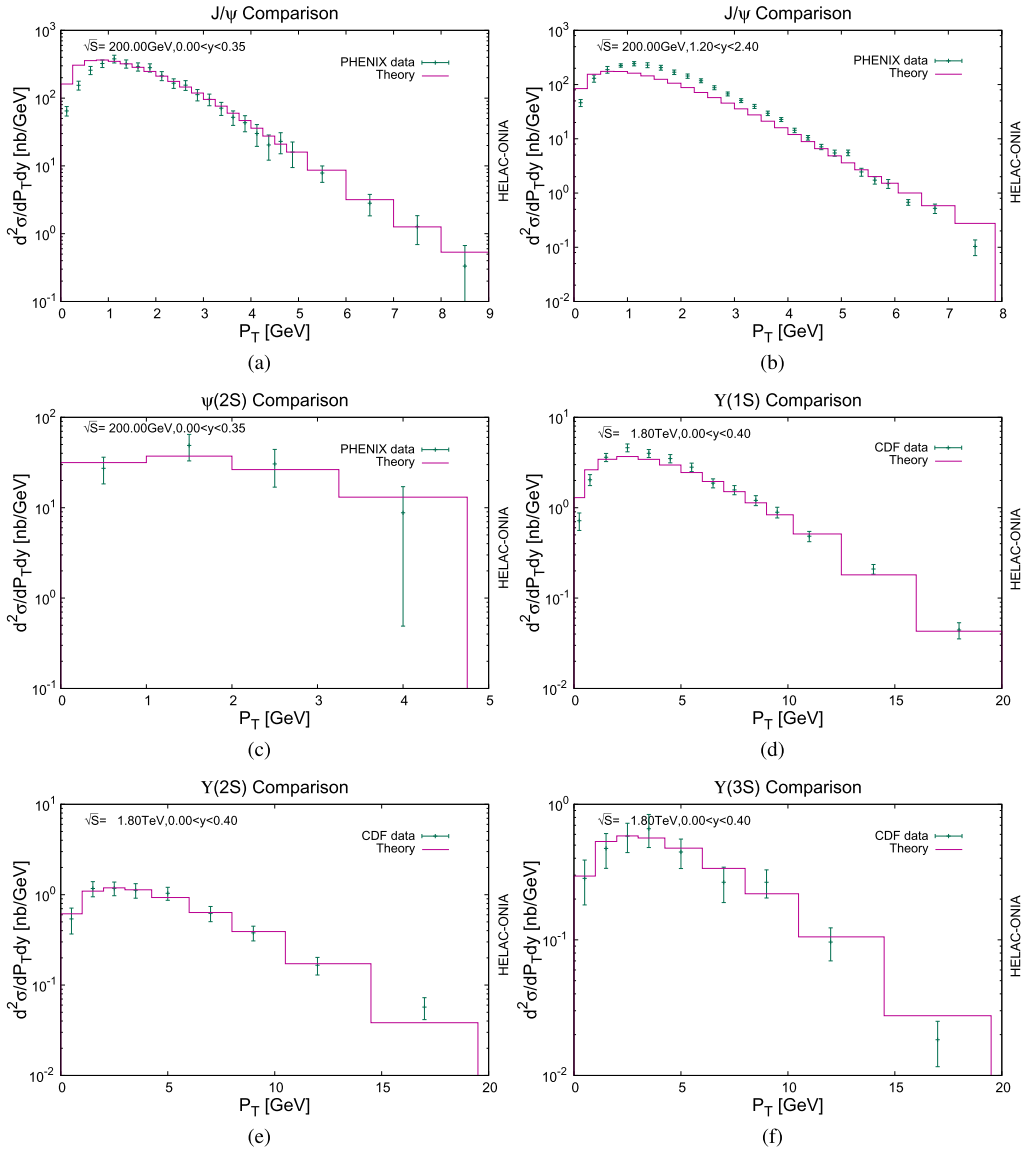

Fig. 1. Comparisons with the PHENIX measurements [51] for J/ψ (a, b) and $\psi(2S)$ (c) production and with the CDF measurements [52] for $\Upsilon(1S)$ (d), $\Upsilon(2S)$ (e) and $\Upsilon(3S)$ (f) production.

In contrast, there is no differential measurement of Υ yields at RHIC. There exists data from the fixed-target Fermilab experiment E866 [55] but only at low P_T. We therefore performed a fit of $d^2\sigma/dP_T dy$ to CDF [52] Run I data at $\sqrt{s} = 1.8$ TeV. The results for Υ are presented in Table 2b having fixed $n = 2$ and $\langle P_T \rangle = 13.5$ GeV. For illustration, the comparisons between the fit and the CDF data [52] are shown in Fig. 1d–f. Some comments about the fit are however in order. If we instead performed a combined fit to CDF [52], ATLAS [56], CMS [57] and LHCb [58,59] data, the value of κ (λ) would be shifted by at most 30% (10%) but with significantly worse χ^2.

Table 3
Various decays (and branching ratios) considered in this article [63].

Decay channel	Branching ratio (%)
$\psi(2S) \to J/\psi + X$	57.4
$\Upsilon(2S) \to \Upsilon(1S) + X$	30.2
$\Upsilon(3S) \to \Upsilon(1S) + X$	8.92
$\Upsilon(3S) \to \Upsilon(2S) + X$	10.6

(a) Decay within a family

Decay channel	Branching ratio (%)
$J/\psi \to \mu^+\mu^-$	5.93
$\psi(2S) \to \mu^+\mu^-$	0.75
$\Upsilon(1S) \to \mu^+\mu^-$	2.48
$\Upsilon(2S) \to \mu^+\mu^-$	1.93
$\Upsilon(3S) \to \mu^+\mu^-$	2.18

(b) Leptonic decays

All this may however not be so relevant since, as for the charmonia, the fit to TeV data tend to underestimate the RHIC P_T-integrated Υ production cross section as measured by STAR [60] by a factor a bit smaller than 2 – the STAR result has however a 30% uncertainty. The uncertainties on κ and λ given by the χ^2 fit are therefore far too optimistic since the Crystall Ball parametrisation seems not to correctly capture the energy dependence of the cross section. The corresponding DPS yields of Υ at AFTER@LHC which we give here should therefore be considered as conservative *lower* estimates. All of the above fits are performed with MSTW2008NLO PDF set [61] available in LHAPDF5 [62] and the factorisation scale $\mu_F = \sqrt{M_{\mathcal{Q}}^2 + P_T^2}$. The physical mass $M_{\mathcal{Q}}$ for quarkonium is taken from PDG data [63] as well as the branching ratios.

2.2. Single-parton scatterings

2.2.1. Double-charmonium and double-bottomonium production

The SPS contribution to J/ψ-pair production have systematically been investigated in our previous works [16,18]. We have shown that a leading order (LO) calculation in the strong coupling constant, α_s, is enough to account for the low-P_T data as well as the P_T-integrated cross section, the bulk of the events lying at low P_T. However, if one goes to mid P_T (*e.g.* $P_T > 5$ GeV), $\mathcal{O}(\alpha_s^5)$ contributions start to be large. As a consequence, the yield and the polarisation change significantly compared to a LO calculation. Since we are only interested in the data which are measurable with up to 20 fb^{-1} in order to assess the feasibility of measuring quarkonium-pair production with AFTER@LHC, we will focus on the low P_T region. As we will explicitly show, LO evaluations happen to be sufficient. Besides, the colour-octet contributions are also negligible at low P_T for they are suppressed by powers of v without any kinematical enhancement at variance with the single-quarkonium-production case.

On the contrary, the feed-down contributions from higher excited spin-triplet S-wave quarkonium have to be considered. They are substantial as already shown for the J/ψ-pair production in Ref. [18]. These will systematically be taken into account in our predictions as done in Ref. [18]. The branching ratios that will be used in this context are taken from PDG [63] and we have listed them in Table 3 for completeness.

The general formula for the amplitude of the production of a pair of colour-singlet (CS) S-wave quarkonia $\mathcal{Q}_1$ and Q_2 with as initial partons a and b is

$$\begin{aligned}
&\mathcal{A}_{ab\to\mathcal{Q}_1^{\lambda_1}(P_1)+\mathcal{Q}_2^{\lambda_2}(P_2)+X} \\
&\quad= \sum_{s_1,s_2,c_1,c_2} \sum_{s_3,s_4,c_3,c_4} \frac{N(\lambda_1|s_1,s_2)N(\lambda_2|s_3,s_4)}{\sqrt{M_{\mathcal{Q}_1} M_{\mathcal{Q}_2}}} \\
&\qquad\times \frac{\delta_{c_1c_2}\delta_{c_3c_4}}{N_c} \frac{R_1(0)R_2(0)}{4\pi} \mathcal{A}_{ab\to Q_{c_1}^{s_1}\bar{Q}_{c_2}^{s_2}(\mathbf{p}_1=\mathbf{0})+Q_{c_3}^{s_3}\bar{Q}_{c_4}^{s_4}(\mathbf{p}_2=\mathbf{0})+X},
\end{aligned} \tag{10}$$

Table 4
The radial wave functions at the origin squared $|R(0)|^2$ [64] of S-wave quarkonium used in this article.

Quarkonium	$\lvert R(0)\rvert^2$ (GeV^3)
J/ψ	0.81
$\psi(2S)$	0.529
$\Upsilon(1S)$	6.477
$\Upsilon(2S)$	3.234
$\Upsilon(3S)$	2.474

where we denote the momenta of quarkonia $\mathcal{Q}_1$ and $\mathcal{Q}_2$ as P_1 and P_2 respectively and their polarisations as $\lambda_{1,2}$, $N(\lambda_{1,2}|s_{1,3}, s_{2,4})$ are the two spin projectors and $R_{1,2}(0)$ are the radial wave functions at the origin in the configuration space for both quarkonia. In the above equation, we have defined the heavy-quark momenta to be $q_{1,2,3,4}$ such that $P_{1,2} = q_{1,3} + q_{2,4}$ and $p_{1,2} = (q_{1,3} - q_{2,4})/2$. $s_{1,2,3,4}$ are then the heavy-quark spin components and $\delta_{c_i c_j}/\sqrt{N_c}$ is the colour projector. The spin-triplet projector $N(\lambda|s_i, s_j)$ has, in the non-relativistic limit, $v \to 0$, the following expression

$$N(\lambda|s_i, s_j) = \frac{\varepsilon_\mu^\lambda}{2\sqrt{2}M_{\mathcal{Q}}}\bar{v}(\frac{\mathbf{P}}{2}, s_j)\gamma^\mu u(\frac{\mathbf{P}}{2}, s_i). \tag{11}$$

All these computations can be performed automatically in the HELAC-ONIA [53] framework based on recursion relations. The radial wave functions at the origin $R(0)$ are taken from Ref. [64], which were derived in the QCD-motivated Buchmüller-Tye potential [65]. We also listed their values in Table 4.

2.2.2. Charmonium–bottomonium pair production

The simultaneous production of a charmonium and a bottomonium has been studied in Refs. [13,19]. Its CSM contributions are expected to be suppressed because the direct LO contributions in CS mechanism (CSM) are $\mathcal{O}(\alpha_s^6)$, *i.e.* α_s^2 suppressed compared to double-charmonium and double-bottomonium production. Hence, it is expected to be a golden channel to probe colour-octet mechanism (COM) at the LHC [13]. However, such a statement is valid only if one can clearly separate DPS and SPS events experimentally since the DPS contributions would be substantial. For a thorough discussion, the reader is guided to [19]. In contrast, colour-octet (CO) contributions can appear at $\mathcal{O}(\alpha_s^4)$, which however are suppressed by the small size of the CO long distance matrix elements (LDMEs). If one follows the arguments of Ref. [13], one is entitled to consider only the $c\bar{c}(^3S_1^{[8]}) + b\bar{b}(^3S_1^{[8]})$, $c\bar{c}(^3S_1^{[1]}) + b\bar{b}(^3S_1^{[8]})$ and $c\bar{c}(^3S_1^{[8]}) + b\bar{b}(^3S_1^{[1]})$ channels. This approximation is however based on the validity of the velocity scaling rules of the LMDEs which may not be reliable. A complete computation – even at LHC energies – accounting for all the possible channels up to v^7 in NRQCD is still lacking in the literature: there are indeed more than 50 channels at LO in α_s contributing to $\psi + \Upsilon$ production. Thanks to the automation of HELAC-ONIA [53,54], such a complete evaluation is at reach.

The formula for the S-wave CO amplitude is similar to that for CS state production with the following formal replacements for CO in Eq. (10)

$$\frac{\delta_{c_i,c_j}}{\sqrt{N_c}} \to \sqrt{2}T^a_{c_i c_j}, \frac{R_i(0)}{\sqrt{4\pi}} \to \frac{\sqrt{\langle \mathcal{O}^i(^{2s+1}S_J^{[8]})\rangle}}{\sqrt{(2J+1)(N_c^2-1)}}, \tag{12}$$

where $T^a_{c_i c_j}$ is the Gell-Mann matrix and $\langle \mathcal{O}^i(^3S_1^{[8]})\rangle$ is the CO LDME. We refer the reader to Ref. [53] for the P-wave amplitudes.

The non-perturbative CO LDMEs should be determined from experimental data. Their values unfortunately depend much on the fit procedures. We took four sets of LDMEs from the literature (see the details in Appendix A.2).

Finally, we describe our parameters for our SPS calculations. In the non-relativistic limit, the mass of the heavy quarkonium can be expressed as the sum of the corresponding heavy-quark-pair masses. In our case, we have

$$M_{\mathcal{Q}} = 2m_Q, \tag{13}$$

where $m_Q = m_c$ for charmonium and $m_Q = m_b$ for bottomonium. The masses of charm quark and bottom quark are taken as $m_c = 1.5 \pm 0.1$ GeV and $m_b = 4.75 \pm 0.25$ GeV. The factorisation scale μ_F and the renormalisation scale μ_R are taken as $\mu_F = \mu_R \in [\frac{1}{2}\mu_0, 2\mu_0]$ with $\mu_0 = \sqrt{(M_{\mathcal{Q}_1} + M_{\mathcal{Q}_2})^2 + P_T^2}$. The advantage of using $\mu_0 = \sqrt{(M_{\mathcal{Q}_1} + M_{\mathcal{Q}_2})^2 + P_T^2}$ is that we are able to recover the correct mass threshold $M_{\mathcal{Q}_1} + M_{\mathcal{Q}_2}$ in the low P_T regime. Finally, the PDF set for the SPS calculation is CTEQ6L1 [66] with the one-loop renormalisation group running of α_s.

3. Energy dependence of the ratio DPS over SPS

Due to the very large integrated luminosity of AFTER@LHC (up to 20 fb^{-1} per year) compared to the experiments performed at RHIC, the measurement of double-quarkonium production at AFTER@LHC will provide a unique test of the interplay between the DPS and SPS production mechanisms in a new energy range. The energy dependence of σ_{eff} will be explored at a wide energy range when combined with the LHC collider and Tevatron data.[3] Due to the double enhancement of the initial gluon–gluon luminosity with the energy, $\sqrt{s}$, DPS contributions are expected to be more and more important with respect to the SPS ones at larger $\sqrt{s}$. This can be observed on Fig. 2.

One however sees on Fig. 2 that a change of σ_{eff} from 15 mb – which seems to be the favoured value for jet-related observables – to 5 mb – which is the value extracted by D0 from the $J/\psi + J/\psi$ data [7] – results in a significant change in the point where both contributions are equal. In the latter case, it occurs very close to the energy of AFTER@LHC, in the former case, it occurs between the Tevatron and the LHC energies. All this clearly motivates for measurement and σ_{eff} extractions at low energies.

4. Impact of the QCD corrections at low transverse momenta

Before showing our results and in order to motivate the use of LO predictions for this exploratory study, we have found it useful to give an explicit comparison between the differential cross section at LO and NLO* for double-J/ψ production in the kinematical domain accessible with 20 fb^{-1}, that is up to transverse momenta on the order of 10 GeV at the very most. Indeed,

[3] Since we noted that the energy dependence obtained with the partonic amplitude ($gg \to \mathcal{Q}X$) given by a Crystal Ball fit with fixed parameters is not optimal when going to TeV energies down to RHIC energies, we have used the fit parameters of [20] (based on a fit of Tevatron and LHC data) to predict the DPS yield in the TeV range and our fit to the PHENIX data for the RHIC and fixed-target-experiment energy range.

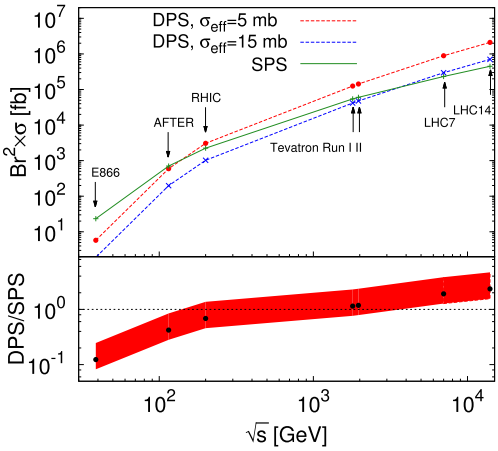

Fig. 2. (Upper panel) The cross sections of (prompt-)J/ψ pair production via SPS and DPS mechanisms for two values of $\sigma_{\rm eff}$ as a function of $\sqrt{s}$. (Lower panel) DPS over SPS yield ratio for $5 < \sigma_{\rm eff} < 15$ mb. The black circles correspond to 10 mb. [Aside from the choice of $\sigma_{\rm eff}$, no theoretical uncertainties are included.]

in a previous study [16], we have showed that the impact of the real-emission corrections, such as $gg \to J/\psi + J/\psi + g$, becomes increasingly important at large transverse momenta.

Figs. 3 show the comparison between LO results and NLO* results (which are known to reproduce well the full NLO [17]). The invariant-mass and rapidity-difference spectra are not affected by the real emission at α_S^5. Indeed, in the low-P_T region, the Born topologies are dominant, and there is no kinematical enhancement in the real-emission topologies which could compensate the α_S suppression. Only when one goes to large transverse momenta, these are enhanced and can become dominant. This explains the difference in the slope as a function of the leading P_T in Fig. 3c. The results are however similar for $P_T < 10$ GeV where the cross sections are larger than 0.1 fb.

In addition, as we already discussed in Ref. [18], at LO, a $2 \to 2$ kinematics for SPS would result in a transverse momentum of the J/ψ-pair $P_T^{\psi\psi}$ being zero and in a trivial LO distribution on Fig. 3d. This is however not the case if one takes into account a possible intrinsic k_T of the initial partons which can also been considered as a part of QCD radiative corrections – initial-state radiations to be precise. Such a smearing can phenomenologically be accounted for and compared to a pQCD result. To do so, we have smeared the kinematics of LO events using a Gaussian distribution with $\langle k_T \rangle = 1$ & 2 GeV as done in Refs. [16,18]. We stress that the value of $\langle k_T \rangle$ is essentially empirical, hence the choice of two values for illustration (resp. curves labelled sm1 and sm2). This can thus be compared with our NLO* curves in the accessible domain with $\mathcal{O}(20)$ fb^{-1} at AFTER@LHC, that is $P_T^{\psi\psi} < 10$ GeV. One sees that the smearing mimics relatively well the effect of the QCD corrections with $\langle k_T \rangle = 2$ GeV which we will use in the following for the comparison with the DPS yield. Overall, the $P_T^{\psi\psi}$ distribution is obviously very different than a single peak at 0.

5. Predictions at AFTER@LHC

We are now in the position to present our numerical results at $\sqrt{s} = 115$ GeV in $p + p$ collisions. The total cross section we obtained are given in Tables 5, 6 and 7. The results have been

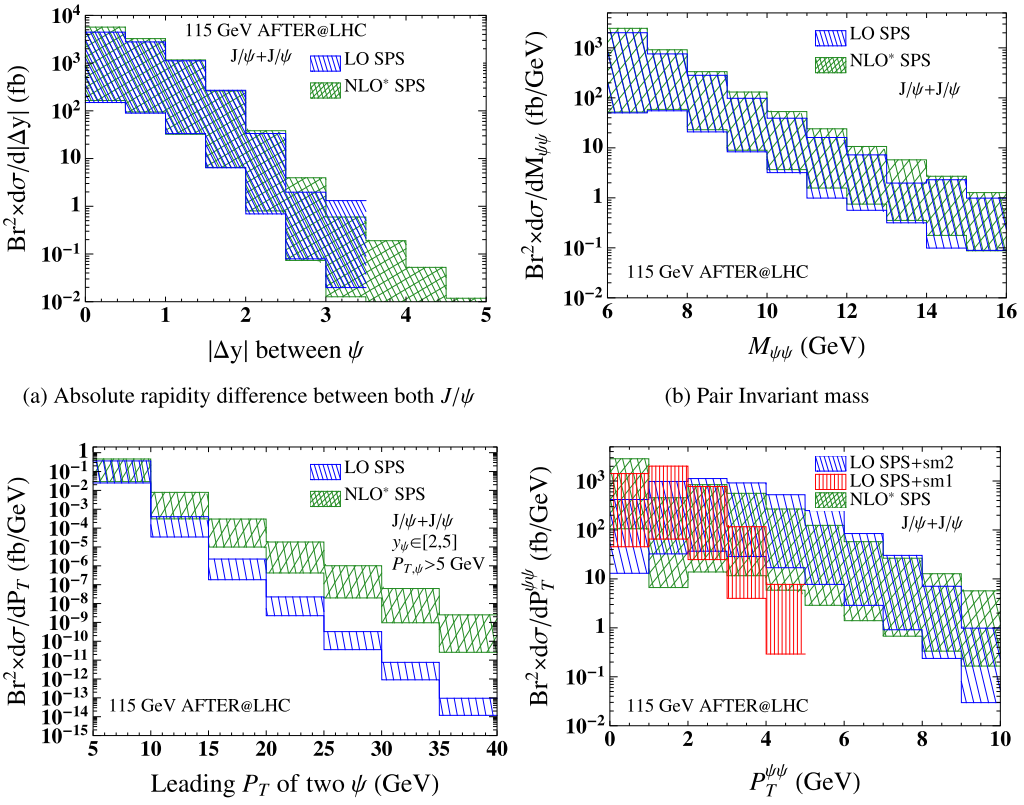

(a) Absolute rapidity difference between both J/ψ

(b) Pair Invariant mass

(c) Leading P_T among the J/ψ pair

(d) Pair transverse momentum

Fig. 3. LO vs. NLO* differential distributions.

multiplied by the branching ratios into a muon pair and they are all in unit of fb. In general, we have

$$\sigma^{\Upsilon\Upsilon\to 4\mu} \ll \sigma^{\psi\Upsilon\to 4\mu} \ll \sigma^{\psi\psi\to 4\mu}. \tag{14}$$

The DPS contributions decrease quickly when the mass threshold $M_{\mathcal{Q}_1} + M_{\mathcal{Q}_2}$ increases because of its square dependence of the initial-state parton luminosity. With the nominal integrated luminosity of 20 fb^{-1} proposed to be collected at AFTER@LHC, we find that the measurement double-bottomonium production is out of reach[4] and one may be able to record a few $J/\psi + \Upsilon(1S)$ events, which receives substantial DPS contributions.

One should however always keep in mind that $\sigma_{\rm SPS}$ for $\psi + \Upsilon$ production strongly depends on the CO LDMEs. We have investigated this dependence in Appendix A.2 with four different sets of LDMEs and the results vary up to one order of magnitude which precludes any strong conclusions.[5] In addition, these LDMEs are usually fit from the experimental data at high transverse momentum region and are known to overestimate the single-quarkonium yields at low P_T

[4] We note that such a measurement has never been done anywhere else.

[5] For convenience and possible future studies, we have tabulated in Appendix A.1 the values of all the relevant short-distance coefficients which can then be combined with any LDME set.

Table 5
$\sigma(pp \to \mathcal{Q}_1 + \mathcal{Q}_2 + X) \times \mathcal{B}(\mathcal{Q}_1 \to \mu^+\mu^-)\mathcal{B}(\mathcal{Q}_2 \to \mu^+\mu^-)$ in units of fb at $\sqrt{s} = 115$ GeV, where $\mathcal{Q}_1, \mathcal{Q}_2 = J/\psi, \psi(2S)$. The DPS uncertainties are from $\sigma_{\rm eff}$ and the SPS ones from m_Q and the scales.

	$J/\psi + J/\psi$	$J/\psi + \psi(2S)$	$\psi(2S) + \psi(2S)$
$\sigma_{\rm DPS}$	590^{+730}_{-210}	$19^{+23}_{-6.7}$	$0.15^{+0.18}_{-0.052}$
$\sigma_{\rm SPS}^{\rm CSM}$	700^{+3600}_{-560}	85^{+440}_{-68}	$2.5^{+13}_{-2.0}$

Table 6
$\sigma(pp \to \mathcal{Q}_1 + \mathcal{Q}_2 + X) \times \mathcal{B}(\mathcal{Q}_1 \to \mu^+\mu^-)\mathcal{B}(\mathcal{Q}_2 \to \mu^+\mu^-)$ in units of fb with $\sqrt{s} = 115$ GeV, where $\mathcal{Q}_1 = J/\psi, \psi(2S)$ and $\mathcal{Q}_2 = \Upsilon(1S), \Upsilon(2S), \Upsilon(3S)$. For SPS production, only the upper limits of the yields are given (see text). The DPS uncertainties are from $\sigma_{\rm eff}$.

	$J/\psi + \Upsilon(1S)$	$J/\psi + \Upsilon(2S)$	$J/\psi + \Upsilon(3S)$
$\sigma_{\rm DPS}$	$0.17^{+0.21}_{-0.058}$	$0.037^{+0.045}_{-0.013}$	$0.018^{+0.023}_{-0.0063}$
$\sigma_{\rm SPS}^{\rm NRQCD}$	< 0.69	< 0.14	< 0.11
	$\psi(2S) + \Upsilon(1S)$	$\psi(2S) + \Upsilon(2S)$	$\psi(2S) + \Upsilon(3S)$
$\sigma_{\rm DPS}$	$2.6 \cdot 10^{-3}\ ^{+3.2\cdot10^{-3}}_{-9.1\cdot10^{-4}}$	$5.7 \cdot 10^{-4}\ ^{+6.9\cdot10^{-4}}_{-2.0\cdot10^{-4}}$	$2.8 \cdot 10^{-4}\ ^{+3.4\cdot10^{-4}}_{-9.8\cdot10^{-5}}$
$\sigma_{\rm SPS}^{\rm NRQCD}$	< 0.031	$< 5.4 \cdot 10^{-3}$	$< 3.0 \cdot 10^{-3}$

Table 7
$\sigma(pp \to \mathcal{Q}_1 + \mathcal{Q}_2 + X) \times \mathcal{B}(\mathcal{Q}_1 \to \mu^+\mu^-)\mathcal{B}(\mathcal{Q}_2 \to \mu^+\mu^-)$ in units of fb with $\sqrt{s} = 115$ GeV, where $\mathcal{Q}_1, \mathcal{Q}_2 = \Upsilon(1S), \Upsilon(2S), \Upsilon(3S)$. The DPS uncertainties are from $\sigma_{\rm eff}$ and the SPS ones from the m_Q and the scales.

	$\Upsilon(1S) + \Upsilon(1S)$	$\Upsilon(2S) + \Upsilon(2S)$	$\Upsilon(3S) + \Upsilon(3S)$
$\sigma_{\rm DPS}$	$1.2 \cdot 10^{-5}\ ^{+1.4\cdot10^{-5}}_{-4.0\cdot10^{-6}}$	$5.6 \cdot 10^{-7}\ ^{+6.8\cdot10^{-7}}_{-1.9\cdot10^{-7}}$	$1.4 \cdot 10^{-7}\ ^{+1.7\cdot10^{-7}}_{-4.7\cdot10^{-8}}$
$\sigma_{\rm SPS}^{\rm CSM}$	$2.8 \cdot 10^{-3}\ ^{+1.3\cdot10^{-2}}_{-2.2\cdot10^{-3}}$	$3.5 \cdot 10^{-4}\ ^{+1.7\cdot10^{-3}}_{-2.8\cdot10^{-4}}$	$2.2 \cdot 10^{-4}\ ^{+1.1\cdot10^{-3}}_{-1.8\cdot10^{-4}}$
	$\Upsilon(1S) + \Upsilon(2S)$	$\Upsilon(1S) + \Upsilon(3S)$	$\Upsilon(2S) + \Upsilon(3S)$
$\sigma_{\rm DPS}$	$5.1 \cdot 10^{-6}\ ^{+6.2\cdot10^{-6}}_{-1.7\cdot10^{-6}}$	$2.5 \cdot 10^{-6}\ ^{+3.0\cdot10^{-6}}_{-8.7\cdot10^{-7}}$	$5.5 \cdot 10^{-7}\ ^{+6.7\cdot10^{-7}}_{-1.9\cdot10^{-7}}$
$\sigma_{\rm SPS}^{\rm CSM}$	$2.0 \cdot 10^{-3}\ ^{+9.3\cdot10^{-3}}_{-1.6\cdot10^{-3}}$	$1.6 \cdot 10^{-3}\ ^{+7.4\cdot10^{-3}}_{-1.3\cdot10^{-3}}$	$5.6 \cdot 10^{-4}\ ^{+2.6\cdot10^{-3}}_{-4.4\cdot10^{-4}}$

(see [67] and references therein). This is also probably the case for quarkonium-pair production especially when they come from single gluon splittings. We have therefore find it only meaningful to show upper limits on $\sigma_{\rm SPS}$ for $\psi + \Upsilon$ production in Table 6. These numbers are in any case at the limit of observability.

The quoted theoretical uncertainties in the tables result from the variation of $\sigma_{\rm eff}$ within 5 ± 2.75 mb for the DPS yields and from the scale uncertainties as well as heavy-quark-mass uncertainties for the SPS yields, as discussed in Section 2.

As regards double-charmonium production, about 10 thousand events could be collected per year – which is more than what has so far been collected by LHCb and CMS. In the analysis of the differential distributions, we therefore only focus on these and, in particular, on J/ψ-pair production. We show three interesting distributions without kinematical cuts. Along the lines of [40], we also used the LHCb kinematical acceptance, *i.e.* the rapidity of J/ψ restricted to be in the interval of $[2, 5]$.

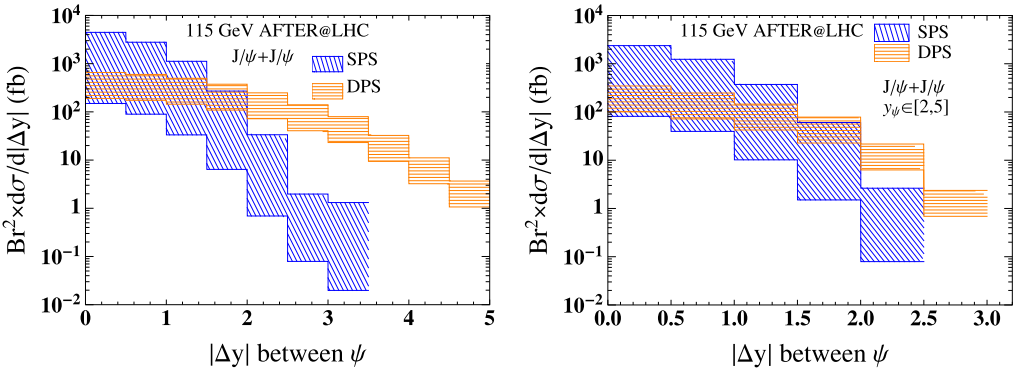

Fig. 4. Differential cross section as a function of the absolute rapidity difference of the J/ψ pair, without (left) or with (right) a rapidity cut.

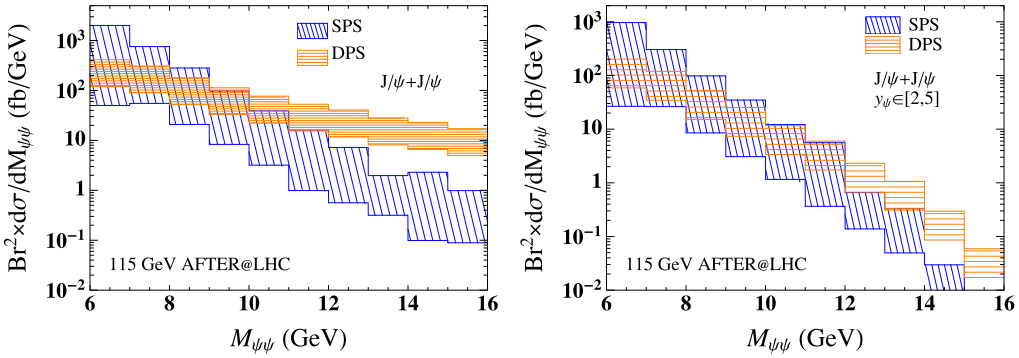

Fig. 5. Differential cross section as a function of the invariant mass of the J/ψ pair, without (left) or with (right) a rapidity cut.

The absolute rapidity difference between the J/ψ pair is expected to be a good observable to discriminate the DPS and SPS contributions. This was first pointed out in Ref. [20] and this was used later on by D0 Collaboration [7] to extract $\sigma_{\rm eff}$ from double-J/ψ production at the Tevatron. The DPS events should have a broader distribution in Δy than the SPS ones, because two (relatively) independent hard interactions happen simultaneously in DPS while the two J/ψ from SPS are more correlated. The situation still does not change at AFTER@LHC without or with cut as Fig. 4 (left) and (right) show. In the latter case, the restriction to negative rapidities in the centre-of-mass obviously reduce the Δy range. Starting from $\Delta y = 2$, the DPS events dominate the SPS events. A ratio DPS/SPS of 10 is obtained for $\Delta y > 2$. The distribution of the invariant mass for the J/ψ pair $M_{\psi\psi}$ reflects a similar information as the Δy distribution. Hence, it follows that the $M_{\psi\psi}$ spectra of DPS are also broader than those of SPS, which can be seen on Fig. 5 (left) and (right).

As we discussed earlier, predictions for the $P_T^{\psi\psi}$ dependence of the SPS yield depend much on the k_T smearing of the initial partons which can mimic a part of the QCD corrections. Due to the relative smaller yields at AFTER@LHC energies than at LHC energies, one can only access $P_T^{\psi\psi} < 10$ GeV, as illustrated on Fig. 6. In such a kinematical region, the k_T smearing effect makes the SPS spectrum as broad as the DPS one with $\langle k_T \rangle = 2$ GeV.

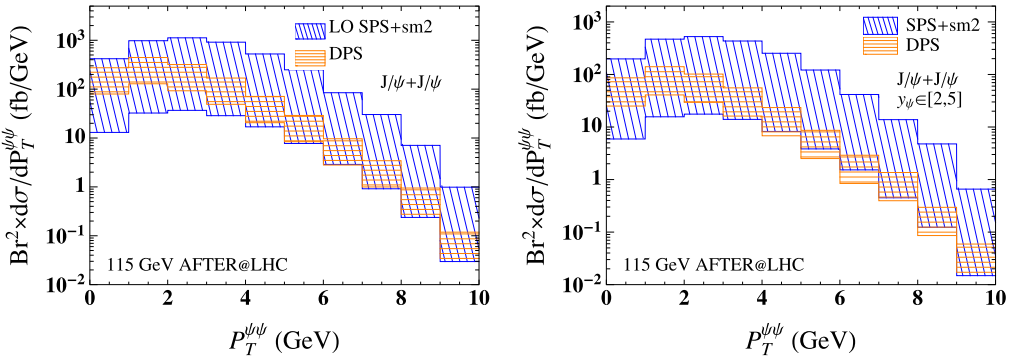

Fig. 6. Differential cross section as a function of the transverse momentum of the J/ψ pair, without (left) or with (right) a rapidity cut.

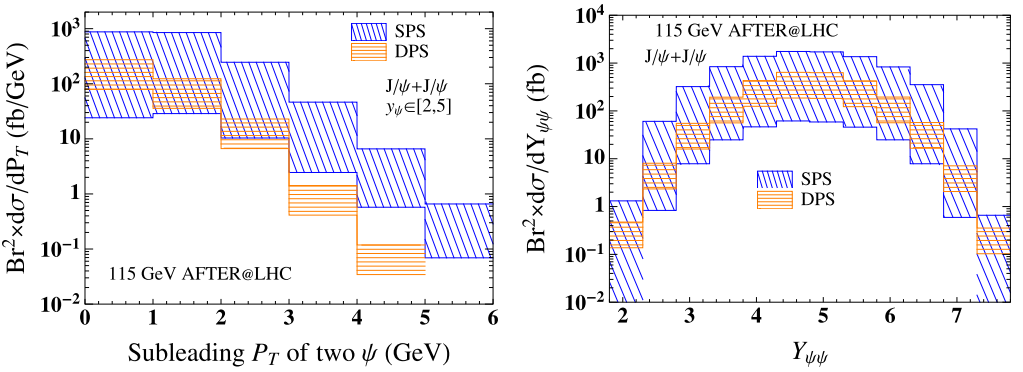

Fig. 7. Differential cross section as a function of (left) the sub-leading P_T with a rapidity cut and (right) the rapidity of the J/ψ pair.

Finally, we present on Fig. 7 the cross section as a function of the total rapidity of the J/ψ pair (right), $Y_{\psi\psi}$, and of the sub-leading P_T between the J/ψ pair (left). One sees that the sub-leading P_T spectrum may be measured up to 6 GeV with AFTER@LHC. As regards the rapidity distribution, its maximum is obviously located at $Y_{\rm cms} = 0$, that is $Y = 4.8$ in the laboratory frame. One sees that one can expect some counts down to $Y_{\psi\psi} \simeq 2.5$ where $x_F \simeq \frac{2M_{\psi\psi}}{\sqrt{s}} \sinh(Y_{\psi\psi} - 4.8) \simeq -0.5$. This is precisely the kinematical region where double intrinsic $c\bar{c}$ coalescence contributes on average [10]. Any modulation in the pair-rapidity distribution would sign the presence of such a contribution.

Finally, we have investigated the impact of using different (double) PDFs (MSTW2008NLO [61], CTEQ6L1 [66], GS09 dPDF [47]) on differential distributions, they are also shown in Fig. 8; they are found to be moderate in all cases.

6. Conclusion

We have discussed double-quarkonium production in proton–proton collisions at a fixed-target experiment using the LHC proton beams, AFTER@LHC. These processes have lately attracted much attention, both in the theorist and experimentalist communities. They are expected to be

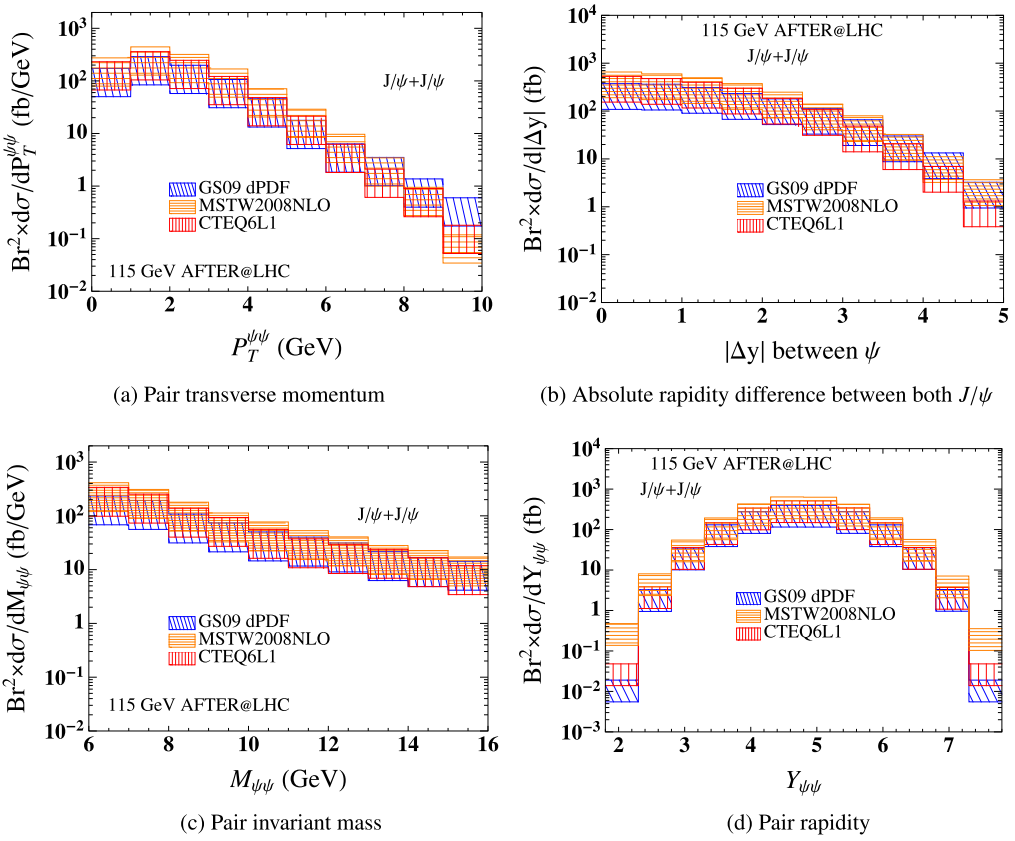

(a) Pair transverse momentum

(b) Absolute rapidity difference between both J/ψ

(c) Pair invariant mass

(d) Pair rapidity

Fig. 8. Differential distributions for DPS with various PDFs: (a) transverse momentum spectrum; (b) absolute rapidity difference; (c) invariant mass distribution; (d) rapidity of J/ψ pair.

good observables to further constrain the various models describing heavy-quarkonium production. Double-quarkonium production also provides a good opportunity to study DPS since the yields of single quarkonium production is large and their decay to four muons is a clean signal at hadron colliders. AFTER@LHC provides very appealing opportunities to study these observables with a LHCb-like detector and in a new energy region.

In this paper, we have studied both DPS and SPS contributions for double-quarkonium production. These processes include $\psi(n_1S)+\psi(n_2S)$, $\psi(n_1S)+\Upsilon(m_1S)$ and $\Upsilon(m_1S)+\Upsilon(m_2S)$ with $n_1, n_2 = 1, 2$ and $m_1, m_2 = 1, 2, 3$. DPS contributions are estimated in a data-driven way, while SPS ones are calculated at LO in non-relativistic QCD (NRQCD) [68], more precisely in the CSM for $\psi(n_1S)+\psi(n_2S)$ and $\Upsilon(m_1S)+\Upsilon(m_2S)$ and accounting for CO contributions for $\psi(n_1S)+\Upsilon(m_1S)$. From our calculations, we find that ten thousand of double-charmonium events can indeed be measured at AFTER@LHC with the yearly integrated luminosity of 20 fb^{-1}. In the most backward region, a careful analysis of the rapidity distribution could also uncover double intrinsic $c\bar{c}$ coalescence contributions. In general, future measurements on double-charmonium production can provide extremely valuable information on QCD, in particular important tests on the factorisation formula for DPS and the energy (in)dependence of $\sigma_{\rm eff}$.

Acknowledgements

This work is supported in part by the France–China Particle Physics Laboratory (FCPPL) and by the French CNRS via the grants PICS-06149 Torino-IPNO, FCPPL-Quarkonium4AFTER & PEPS4AFTER2. H.-S. Shao is also supported by the ERC grant 291377 "LHCtheory: Theoretical predictions and analyses of LHC physics: advancing the precision frontier".

Appendix A. Charmonium–bottomonium pair production in NRQCD

A.1. Short-distance coefficients for charmonium–bottomonium pair production

In NRQCD [68], the cross section for a charmonium $\mathcal{C}$ and a bottomonium $\mathcal{B}$ production can systematically be written as

$$\sigma(\mathcal{C}+\mathcal{B}) = \sum_{n_1,n_2} \sigma(c\bar{c}[n_1] + b\bar{b}[n_2]) \times \langle \mathcal{O}^{\mathcal{C}}(n_1)\rangle \times \langle \mathcal{O}^{\mathcal{B}}(n_2)\rangle, \tag{A.1}$$

where n_1, n_2 are different possible Fock states, $\sigma(c\bar{c}[n_1] + b\bar{b}[n_2])$ is the short-distance coefficient (SDC) for the production of a charm–quark pair in the Fock state n_1 and a bottom-quark pair in the Fock state n_2 simultaneously. The LDMEs $\langle \mathcal{O}^{\mathcal{C}}(n_1)\rangle$ and $\langle \mathcal{O}^{\mathcal{B}}(n_2)\rangle$ should obey the velocity-scaling rules of NRQCD. In this appendix, we give the complete list of the SDCs for charmonium–bottomonium pair production at the leading order in α_s in proton–proton collisions at the centre-of-mass energy of $\sqrt{s} = 115$ GeV. This includes the contributions from ${}^3S_1^{[1]}$, ${}^3S_1^{[8]}$, ${}^1S_0^{[8]}$, ${}^3P_J^{[8]}$ $(J = 0, 1, 2)$ for S-wave quarkonium production and from ${}^3S_1^{[8]}$, ${}^3P_J^{[1]}$ $(J = 0, 1, 2)$ for P-wave quarkonium production. There are in total 66 non-vanishing channels to be computed. Such a computation is automatic in HELAC-Onia [53,54], but has never been carried out even at LHC energies. Thanks to the heavy-quark-spin symmetry of NRQCD, we have

$$\langle \mathcal{O}^{\mathcal{C},\mathcal{B}}({}^3P_J^{[8]})\rangle = (2J+1) \times \langle \mathcal{O}^{\mathcal{C},\mathcal{B}}({}^3P_0^{[8]})\rangle. \tag{A.2}$$

We can thus define new SDCs relevant for ${}^3P_J^{[8]}$

$$\begin{aligned}
\sigma(c\bar{c}[\sum_{J=0}^{2} {}^3P_J^{[8]}] + b\bar{b}[n_2]) &\equiv \sum_{J=0}^{2} (2J+1) \times \sigma(c\bar{c}[{}^3P_J^{[8]}] + b\bar{b}[n_2]),\\
\sigma(c\bar{c}[n_1] + b\bar{b}[\sum_{J=0}^{2} {}^3P_J^{[8]}]) &\equiv \sum_{J=0}^{2} (2J+1) \times \sigma(c\bar{c}[n_1] + b\bar{b}[{}^3P_J^{[8]}]).
\end{aligned} \tag{A.3}$$

Therefore, we have

$$\begin{aligned}
&\sum_{J=0}^{2} \sigma(c\bar{c}[{}^3P_J^{[8]}] + b\bar{b}[n_2]) \times \langle \mathcal{O}^{\mathcal{C}}({}^3P_J^{[8]})\rangle \langle \mathcal{O}^{\mathcal{B}}(n_2)\rangle\\
&\quad = \sigma(c\bar{c}[\sum_{J=0}^{2} {}^3P_J^{[8]}] + b\bar{b}[n_2]) \times \langle \mathcal{O}^{\mathcal{C}}({}^3P_0^{[8]})\rangle \langle \mathcal{O}^{\mathcal{B}}(n_2)\rangle,
\end{aligned}$$

Table A.8
The SDCs (at the leading order in α_s) for the various combinations of the Fock states contributing to charmonium–bottomonium pair production at $\sqrt{s} = 115$ GeV. The unit of the SDCs of $c\bar{c}[n_1] + b\bar{b}[n_2]$ is fb/GeV$^{6+2L_1+2L_2}$, where $L_i = 0$ when n_i is S-wave and $L_i = 1$ when n_i is P-wave. The uncertainty quoted is coming from the variation of $\mu_F = \mu_R \in [\frac{1}{2}\mu_0, 2\mu_0]$ ($\mu_0 = \sqrt{4(m_c + m_b)^2 + P_T^2}$) and the uncertainties on $m_c = 1.5 \pm 0.1$ GeV and $m_b = 4.75 \pm 0.25$ GeV.

Fock state	$b\bar{b}[^3S_1^{[1]}]$	$b\bar{b}[^3S_1^{[8]}]$	$b\bar{b}[^1S_0^{[8]}]$	$b\bar{b}[\sum_{J=0}^{2}{}^3P_J^{[8]}]$	$b\bar{b}[^3P_0^{[1]}]$	$b\bar{b}[^3P_1^{[1]}]$	$b\bar{b}[^3P_2^{[1]}]$
$c\bar{c}[^3S_1^{[1]}]$	–	13^{+63}_{-10}	–	–	–	–	–
$c\bar{c}[^3S_1^{[8]}]$	40^{+200}_{-32}	770^{+4000}_{-620}	2700^{+14000}_{-2200}	720^{+4200}_{-590}	160^{+950}_{-130}	$7.3^{+44.0}_{-6.0}$	43^{+250}_{-36}
$c\bar{c}[^1S_0^{[8]}]$	–	220^{+1100}_{-170}	650^{+3500}_{-520}	180^{+1100}_{-150}	46^{+280}_{-38}	$2.0^{+12}_{-1.6}$	$9.1^{+56}_{-7.6}$
$c\bar{c}[\sum_{J=0}^{2}{}^3P_J^{[8]}]$	–	470^{+2700}_{-380}	1200^{+7500}_{-990}	330^{+2400}_{-280}	$31^{+220}_{-26.0}$	$1.2^{+8.6}_{-1.}$	$8.^{+58}_{-6.8}$
$c\bar{c}[^3P_0^{[1]}]$	–	31^{+180}_{-25}	210^{+1300}_{-180}	25^{+180}_{-21}	12^{+87}_{-10}	$0.37^{+2.6}_{-0.31}$	$3.1^{+23}_{-2.7}$
$c\bar{c}[^3P_1^{[1]}]$	–	21^{+130}_{-18}	69^{+430}_{-57}	$7.5^{+54}_{-6.4}$	$3.6^{+26}_{-3.1}$	$0.33^{+2.3}_{-0.28}$	$1.0^{+7.2}_{-0.86}$
$c\bar{c}[^3P_2^{[1]}]$	–	21^{+120}_{-18}	7.5^{+310}_{-40}	$6.1^{+44}_{-5.2}$	$3.0^{+22}_{-2.5}$	$0.15^{+1.1}_{-0.13}$	$0.79^{+5.8}_{-0.68}$

$$\sum_{J=0}^{2} \sigma(c\bar{c}[n_1] + b\bar{b}[^3P_J^{[8]}]) \times \langle \mathcal{O}^{\mathcal{C}}(n_1)\rangle \langle \mathcal{O}^{\mathcal{B}}(^3P_J^{[8]})\rangle$$
$$= \sigma(c\bar{c}[n_1] + b\bar{b}[\sum_{J=0}^{2} {}^3P_J^{[8]}]) \times \langle \mathcal{O}^{\mathcal{C}}(n_1)\rangle \langle \mathcal{O}^{\mathcal{B}}(^3P_0^{[8]})\rangle. \quad \text{(A.4)}$$

We display the numerical values for the SDCs for these Fock states in Table A.8 with CTEQ6L1 [66] as our PDF set.

A.2. Cross sections for single-parton scattering

From the SDCs given in Table A.8 and the LDMEs extracted from the experimental data, we are now able to estimate the cross sections of charmonium + bottomonium pair production at $\sqrt{s} = 115$ GeV. The values of the LDMEs however significantly differ depending on the different experimental input data and the different fit setup. For example, the CO LDMEs of J/ψ extracted from pp data can be quite different with or without NLO QCD corrections. Here, we will discuss the results based on four sets of LDMEs for charmonia and bottomonia, which can be described as follows:

Set I: This set is based on the LDMEs of J/ψ, $\psi(2S)$ and χ_c presented in Ref. [69] and those of $\Upsilon(1S)$, $\Upsilon(2S)$, $\Upsilon(3S)$ and $\chi_b(1P)$, $\chi_b(2P)$ presented in Ref. [70]. They are extracted from Tevatron data with SDCs at LO in α_s. The LDMEs of $\chi_b(3P)$ have been set to zero in the fit of Ref. [70].[6]

Set II: This set is based on LDMEs of J/ψ, $\psi(2S)$, χ_c, $\Upsilon(1S)$, $\Upsilon(2S)$, $\Upsilon(3S)$, $\chi_b(1P)$, $\chi_b(2P)$ presented in Ref. [72]. The contributions of $\chi_b(3P)$ have been ignored. Hence, we will set the LDMEs of $\chi_b(3P)$ to be zero. The fit was performed at LO in α_s. The LHC, Tevatron and RHIC data were used to perform this combined fit.

[6] Note that both fits used CTEQ5L [71] whereas we have used here CTEQ6L1, whose results are anyhow very close.

Table A.9
$\sigma_{\rm SPS}(pp \to \mathcal{Q}_1 + \mathcal{Q}_2) \times \mathcal{B}(\mathcal{Q}_1 \to \mu^+\mu^-)\mathcal{B}(\mathcal{Q}_2 \to \mu^+\mu^-)$ in units of fb with $\sqrt{s} = 115$ GeV, where $\mathcal{Q}_1 = J/\psi, \psi(2S)$ and $\mathcal{Q}_2 = \Upsilon(1S), \Upsilon(2S), \Upsilon(3S)$ using the four LDME sets discussed in the text. The uncertainty quoted comes only from the SDCs.

	$J/\psi + \Upsilon(1S)$	$J/\psi + \Upsilon(2S)$	$J/\psi + \Upsilon(3S)$
Set I	$0.060^{+0.36}_{-0.050}$	$0.019^{+0.11}_{-0.015}$	$0.016^{+0.095}_{-0.013}$
Set II	$0.095^{+0.60}_{-0.083}$	$0.015^{+0.087}_{-0.022}$	$6.3 \cdot 10^{-3}\ ^{+3.4\cdot10^{-2}}_{-5.1\cdot10^{-3}}$
Set III	$0.077^{+0.47}_{-0.068}$	$0.021^{+0.12}_{-0.018}$	$1.1 \cdot 10^{-2}\ ^{+6.3\cdot10^{-2}}_{-1.0\cdot10^{-2}}$
Set IV	$0.020^{+0.11}_{-0.016}$	$6.0 \cdot 10^{-3}\ ^{+3.4\cdot10^{-2}}_{-4.9\cdot10^{-3}}$	$2.5 \cdot 10^{-3}\ ^{+1.3\cdot10^{-2}}_{-2.0\cdot10^{-3}}$

	$\psi(2S) + \Upsilon(1S)$	$\psi(2S) + \Upsilon(2S)$	$\psi(2S) + \Upsilon(3S)$
Set I	$1.9 \cdot 10^{-3}\ ^{+1.0\cdot10^{-2}}_{-1.5\cdot10^{-3}}$	$5.8 \cdot 10^{-4}\ ^{+3.2\cdot10^{-3}}_{-4.7\cdot10^{-4}}$	$4.6 \cdot 10^{-4}\ ^{+2.6\cdot10^{-3}}_{-3.8\cdot10^{-4}}$
Set II	$4.3 \cdot 10^{-3}\ ^{+2.6\cdot10^{-2}}_{-3.7\cdot10^{-3}}$	$6.8 \cdot 10^{-4}\ ^{+3.9\cdot10^{-3}}_{-1.0\cdot10^{-3}}$	$3.1 \cdot 10^{-4}\ ^{+1.6\cdot10^{-3}}_{-2.5\cdot10^{-4}}$
Set III	$3.2 \cdot 10^{-3}\ ^{+2.0\cdot10^{-2}}_{-2.8\cdot10^{-3}}$	$8.2 \cdot 10^{-4}\ ^{+4.6\cdot10^{-3}}_{-7.3\cdot10^{-4}}$	$4.6 \cdot 10^{-4}\ ^{+2.5\cdot10^{-3}}_{-4.1\cdot10^{-4}}$
Set IV	$9.0 \cdot 10^{-4}\ ^{+4.8\cdot10^{-3}}_{-7.3\cdot10^{-4}}$	$2.8 \cdot 10^{-4}\ ^{+1.5\cdot10^{-3}}_{-2.3\cdot10^{-4}}$	$1.4 \cdot 10^{-4}\ ^{+6.8\cdot10^{-4}}_{-1.1\cdot10^{-4}}$

Set III: This set is based on LDMEs extracted from NLO analyses, *i.e.* the LDMEs of $J/\psi, \psi(2S), \chi_c$ from Ref. [73] and those of $\Upsilon(nS), \chi_b(nP), n = 1, 2, 3$ from Ref. [74]. The CO LDMEs of charmonium are extracted from Tevatron data [73], while both Tevatron data and LHC data were used in Ref. [74].

Set IV: This set is based on LDMEs for charmonium [75] and bottomonium [76] production based on other NLO analyses. They are determined by a combined fit to Tevatron and LHC data.

In order to take into account the feeddown contributions, we have taken the necessary branching ratios from PDG [63]. For the unknown branching ratios, such as $\mathrm{Br}(\chi_b(3P) \to \Upsilon(nS) + \gamma)$, we used the estimated values from Table I of Ref. [74]. The SPS cross sections of $\psi + \Upsilon$ production in proton–proton collisions at $\sqrt{s} = 115$ GeV are presented in Table A.9. As clearly shown, the cross sections significantly differ from one set of LDMEs to another. Before closing this appendix, we would like to stress several points.

- Because some CO LDMEs in Set II and Set IV are negative, the cross sections might be negative, which is of course unphysical. For example, the cross section for direct $J/\psi + \Upsilon(2S)$ production (which then excludes feeddowns) is negative for the Set II and Set IV.
- If one follows the arguments of Ref. [13], one is entitled to consider only the $c\bar{c}(^3S_1^{[8]}) + b\bar{b}[^3S_1^{[8]}]$, $c\bar{c}[^3S_1^{[1]}] + b\bar{b}[^3S_1^{[8]}]$ and $c\bar{c}[^3S_1^{[8]}] + b\bar{b}[^3S_1^{[1]}]$ channels. This approximation is however based on the validity of the velocity-scaling rules of the LMDEs which may not be reliable. By using Set I of LDMEs, we have shown the comparison in Table A.10. The row $^3S_1^{[1]}, ^3S_1^{[8]}$ only include $c\bar{c}(^3S_1^{[8]}) + b\bar{b}[^3S_1^{[8]}]$, $c\bar{c}[^3S_1^{[1]}] + b\bar{b}[^3S_1^{[8]}]$ and $c\bar{c}[^3S_1^{[8]}] + b\bar{b}[^3S_1^{[1]}]$ channels, while the remaining lines contain all CO and CS contributions (with or without feeddown contributions). The results clearly show that the $c\bar{c}(^3S_1^{[8]}) + b\bar{b}[^3S_1^{[8]}]$, $c\bar{c}[^3S_1^{[1]}] + b\bar{b}[^3S_1^{[8]}]$ and $c\bar{c}[^3S_1^{[8]}] + b\bar{b}[^3S_1^{[1]}]$ channels are not sufficient. Moreover, the feeddown contributions are also significant but for $\psi(2S) + \Upsilon(3S)$.

Table A.10
$\sigma_{\rm SPS}(pp \to \mathcal{Q}_1 + \mathcal{Q}_2) \times \mathcal{B}(\mathcal{Q}_1 \to \mu^+\mu^-)\mathcal{B}(\mathcal{Q}_2 \to \mu^+\mu^-)$ in units of fb with $\sqrt{s} = 115$ GeV, where $\mathcal{Q}_1 = J/\psi, \psi(2S)$ and $\mathcal{Q}_2 = \Upsilon(1S), \Upsilon(2S), \Upsilon(3S)$. We have used the Set I of the LDMEs. The uncertainty quoted comes only from the SDCs.

	$J/\psi + \Upsilon(1S)$	$J/\psi + \Upsilon(2S)$	$J/\psi + \Upsilon(3S)$
$\{^3S_1^{[1]}, {}^3S_1^{[8]}\}$	$6.1 \cdot 10^{-3}\ ^{+3.0\cdot10^{-2}}_{-4.9\cdot10^{-3}}$	$1.8 \cdot 10^{-3}\ ^{+8.6\cdot10^{-3}}_{-1.4\cdot10^{-3}}$	$2.5 \cdot 10^{-3}\ ^{+1.2\cdot10^{-2}}_{-2.0\cdot10^{-3}}$
exclude feeddown	$0.024^{+0.15}_{-0.020}$	$6.0 \cdot 10^{-3}\ ^{+3.7\cdot10^{-2}}_{-5.0\cdot10^{-3}}$	$0.011^{+0.065}_{-8.8\cdot10^{-3}}$
include feeddown	$0.060^{+0.36}_{-0.050}$	$0.019^{+0.11}_{-0.015}$	$0.016^{+0.095}_{-0.013}$
	$\psi(2S) + \Upsilon(1S)$	$\psi(2S) + \Upsilon(2S)$	$\psi(2S) + \Upsilon(3S)$
$\{^3S_1^{[1]}, {}^3S_1^{[8]}\}$	$6.1 \cdot 10^{-4}\ ^{+3.0\cdot10^{-3}}_{-4.9\cdot10^{-4}}$	$1.8 \cdot 10^{-4}\ ^{+9.0\cdot10^{-4}}_{-1.5\cdot10^{-4}}$	$2.4 \cdot 10^{-4}\ ^{+1.2\cdot10^{-3}}_{-1.9\cdot10^{-4}}$
exclude feeddown	$1.1 \cdot 10^{-3}\ ^{+6.1\cdot10^{-3}}_{-9.1\cdot10^{-4}}$	$3.0 \cdot 10^{-4}\ ^{+1.6\cdot10^{-3}}_{-2.4\cdot10^{-4}}$	$4.6 \cdot 10^{-4}\ ^{+2.6\cdot10^{-3}}_{-3.8\cdot10^{-4}}$
include feeddown	$1.9 \cdot 10^{-3}\ ^{+1.0\cdot10^{-2}}_{-1.5\cdot10^{-3}}$	$5.8 \cdot 10^{-4}\ ^{+3.2\cdot10^{-3}}_{-4.7\cdot10^{-4}}$	$4.6 \cdot 10^{-4}\ ^{+2.6\cdot10^{-3}}_{-3.8\cdot10^{-4}}$

- The CO LDMEs used in this section are mainly determined by data in the high transverse momentum region. It is important to point out that these LDMEs yield to cross sections overestimating the data in the low transverse momentum region and, hence, the total cross sections for the single quarkonium production (see *e.g.* Ref. [67]). Hence, it is likely that any such NRQCD based estimation of $\psi + \Upsilon$ at low P_T are too optimistic. However, as a conservative estimation, it is reasonable that we consider them as conservation upper limits of the SPS contributions (see Table 6).
- Finally, let us note that the relative importance of pure CO + CO contributions as compared to the mixed CO + CS depends much on the LDME sets. It essentially ranges from 30 to 70 % irrespective of the charmonium–bottomonium pair which is considered. For the sake of completeness, let us add that the pure CS + CS from double feed-down from $\chi_c + \chi_b$ is on the order of a couple of per cent, but for Set IV where it can be up to 10%.

References

[1] N. Brambilla, et al., Heavy quarkonium: progress, puzzles, and opportunities, Eur. Phys. J. C 71 (2011) 1534, arXiv:1010.5827 [hep-ph].

[2] J.P. Lansberg, J/ψ, ψ' and Υ production at hadron colliders: a review, Int. J. Mod. Phys. A 21 (2006) 3857–3916, arXiv:hep-ph/0602091.

[3] A. Andronic, et al., Heavy-flavour and quarkonium production in the LHC era: from proton–proton to heavy-ion collisions, arXiv:1506.03981 [nucl-ex].

[4] ATLAS Collaboration, G. Aad, et al., Measurement of the production cross section of prompt J/ψ mesons in association with a $W^\pm$ boson in pp collisions at $\sqrt{s} = 7$ TeV with the ATLAS detector, J. High Energy Phys. 04 (2014) 172, arXiv:1401.2831 [hep-ex].

[5] ATLAS Collaboration, G. Aad, et al., Observation and measurements of the production of prompt and non-prompt J/ψ mesons in association with a Z boson in pp collisions at $\sqrt{s} = 8$ TeV with the ATLAS detector, Eur. Phys. J. C 75 (5) (2015) 229, arXiv:1412.6428 [hep-ex].

[6] LHCb Collaboration, R. Aaij, et al., Observation of double charm production involving open charm in pp collisions at $\sqrt{s} = 7$ TeV, J. High Energy Phys. 06 (2012) 141, arXiv:1205.0975 [hep-ex];
LHCb Collaboration, R. Aaij, et al., Observation of double charm production involving open charm in pp collisions at $\sqrt{s} = 7$ TeV, J. High Energy Phys. 03 (2014) 108, Addendum.

[7] D0 Collaboration, V.M. Abazov, et al., Observation and studies of double J/ψ production at the Tevatron, Phys. Rev. D 90 (11) (2014) 111101, arXiv:1406.2380 [hep-ex].

[8] V.G. Kartvelishvili, S.M. Esakiya, On hadron induced production of J/ψ meson pairs, Yad. Fiz. 38 (1983) 722–726 (in Russian).
[9] B. Humpert, P. Mery, $\psi\psi$ production at collider energies, Z. Phys. C 20 (1983) 83.
[10] R. Vogt, S.J. Brodsky, Intrinsic charm contribution to double quarkonium hadroproduction, Phys. Lett. B 349 (1995) 569–575, arXiv:hep-ph/9503206.
[11] R. Li, Y.-J. Zhang, K.-T. Chao, Pair production of heavy quarkonium and $B(c)(*)$ mesons at hadron colliders, Phys. Rev. D 80 (2009) 014020, arXiv:0903.2250 [hep-ph].
[12] C.-F. Qiao, L.-P. Sun, P. Sun, Testing charmonium production mechanism via polarized J/ψ pair production at the LHC, J. Phys. G 37 (2010) 075019, arXiv:0903.0954 [hep-ph].
[13] P. Ko, C. Yu, J. Lee, Inclusive double-quarkonium production at the large hadron collider, J. High Energy Phys. 01 (2011) 070, arXiv:1007.3095 [hep-ph].
[14] A.V. Berezhnoy, A.K. Likhoded, A.V. Luchinsky, A.A. Novoselov, Double J/ψ-meson Production at LHC and 4c-tetraquark state, Phys. Rev. D 84 (2011) 094023, arXiv:1101.5881 [hep-ph].
[15] Y.-J. Li, G.-Z. Xu, K.-Y. Liu, Y.-J. Zhang, Relativistic correction to J/ψ and Υ pair production, J. High Energy Phys. 07 (2013) 051, arXiv:1303.1383 [hep-ph].
[16] J.-P. Lansberg, H.-S. Shao, Production of $J/\psi + \eta_c$ versus $J/\psi + J/\psi$ at the LHC: importance of real α_s^5 corrections, Phys. Rev. Lett. 111 (2013) 122001, arXiv:1308.0474 [hep-ph].
[17] L.-P. Sun, H. Han, K.-T. Chao, Impact of J/ψ pair production at the LHC and predictions in nonrelativistic QCD, arXiv:1404.4042 [hep-ph].
[18] J.-P. Lansberg, H.-S. Shao, J/ψ-pair production at large momenta: indications for double-parton scatterings and large α_s^5 contributions, arXiv:1410.8822 [hep-ph].
[19] A.K. Likhoded, A.V. Luchinsky, S.V. Poslavsky, Simultaneous production of charmonium and bottomonium mesons at the LHC, Phys. Rev. D 91 (11) (2015) 114016, arXiv:1503.00246 [hep-ph].
[20] C.H. Kom, A. Kulesza, W.J. Stirling, Pair production of J/ψ as a probe of double parton scattering at LHCb, Phys. Rev. Lett. 107 (2011) 082002, arXiv:1105.4186 [hep-ph].
[21] S.P. Baranov, A.M. Snigirev, N.P. Zotov, Double heavy meson production through double parton scattering in hadronic collisions, Phys. Lett. B 705 (2011) 116–119, arXiv:1105.6276 [hep-ph].
[22] A.V. Berezhnoy, A.K. Likhoded, A.V. Luchinsky, A.A. Novoselov, Double $c\bar{c}$ production at LHCb, Phys. Rev. D 86 (2012) 034017, arXiv:1204.1058 [hep-ph].
[23] S.P. Baranov, A.M. Snigirev, N.P. Zotov, A. Szczurek, W. Schäfer, Interparticle correlations in the production of J/ψ pairs in proton–proton collisions, Phys. Rev. D 87 (3) (2013) 034035, arXiv:1210.1806 [hep-ph].
[24] D. d'Enterria, A.M. Snigirev, Enhanced J/ψ production from double parton scatterings in nucleus–nucleus collisions at the Large Hadron Collider, Phys. Lett. B 727 (2013) 157–162, arXiv:1301.5845 [hep-ph].
[25] D. d'Enterria, A.M. Snigirev, Pair production of quarkonia and electroweak bosons from double-parton scatterings in nuclear collisions at the LHC, Nucl. Phys. A 931 (2014) 303–308, arXiv:1408.5172 [hep-ph].
[26] LHCb Collaboration, R. Aaij, et al., Observation of J/ψ pair production in pp collisions at $\sqrt{s} = 7$ TeV, Phys. Lett. B 707 (2012) 52–59, arXiv:1109.0963 [hep-ex].
[27] CMS Collaboration, V. Khachatryan, et al., Measurement of prompt J/ψ pair production in pp collisions at $\sqrt{s} =$ 7 TeV, J. High Energy Phys. 09 (2014) 094, arXiv:1406.0484 [hep-ex].
[28] S.J. Brodsky, F. Fleuret, C. Hadjidakis, J.P. Lansberg, Physics opportunities of a fixed-target experiment using the LHC beams, Phys. Rep. 522 (2013) 239–255, arXiv:1202.6585 [hep-ph].
[29] J.P. Lansberg, S.J. Brodsky, F. Fleuret, C. Hadjidakis, Quarkonium physics at a fixed-target experiment using the LHC beams, Few-Body Syst. 53 (2012) 11–25, arXiv:1204.5793 [hep-ph].
[30] T. Liu, B.-Q. Ma, Azimuthal asymmetries in lepton-pair production at a fixed-target experiment using the LHC beams (AFTER), Eur. Phys. J. C 72 (2012) 2037, arXiv:1203.5579 [hep-ph].
[31] D. Boer, C. Pisano, Polarized gluon studies with charmonium and bottomonium at LHCb and AFTER, Phys. Rev. D 86 (2012) 094007, arXiv:1208.3642 [hep-ph].
[32] G. Chen, X.-G. Wu, J.-W. Zhang, H.-Y. Han, H.-B. Fu, Hadronic production of Ξ_{cc} at a fixed-target experiment at the LHC, Phys. Rev. D 89 (7) (2014) 074020, arXiv:1401.6269 [hep-ph].
[33] K. Kanazawa, Y. Koike, A. Metz, D. Pitonyak, Transverse single-spin asymmetries in proton–proton collisions at the AFTER@LHC experiment, arXiv:1502.04021 [hep-ph].
[34] R.E. Mikkelsen, A.H. Sørensen, U.I. Uggerhøj, Bremsstrahlung from relativistic heavy ions in a fixed target experiment at the LHC, arXiv:1503.06621 [nucl-ex].
[35] V.P. Goncalves, W.K. Sauter, η_c production in photon-induced interactions at a fixed target experiment at LHC as a probe of the Odderon, Phys. Rev. D 91 (9) (2015) 094014, arXiv:1503.05112 [hep-ph].
[36] J.P. Lansberg, L. Szymanowski, J. Wagner, Lepton-pair production in ultraperipheral collisions at AFTER@LHC, arXiv:1504.02733 [hep-ph].

[37] F.A. Ceccopieri, Studies of backward particle production with a fixed-target experiment using the LHC beams, arXiv:1503.05813 [hep-ph].

[38] M. Anselmino, U. D'Alesio, S. Melis, Transverse single-spin asymmetries in proton–proton collisions at the AFTER@LHC experiment in a TMD factorisation scheme, arXiv:1504.03791 [hep-ph].

[39] F. Lyonnet, A. Kusina, T. Ježo, K. Kovarík, F. Olness, I. Schienbein, J.-Y. Yu, On the intrinsic bottom content of the nucleon and its impact on heavy new physics at the LHC, J. High Energy Phys. 07 (2015) 141, arXiv:1504.05156 [hep-ph].

[40] L. Massacrier, B. Trzeciak, F. Fleuret, C. Hadjidakis, D. Kikola, J.P. Lansberg, H.S. Shao, Feasibility studies for quarkonium production at a fixed-target experiment using the LHC proton and lead beams (AFTER@LHC), arXiv:1504.05145 [hep-ex].

[41] E. Uggerhøj, U.I. Uggerhøj, Strong crystalline fields: a possibility for extraction from the LHC, Nucl. Instrum. Methods B234 (2005) 31–39.

[42] C. Barschel, Precision luminosity measurement at LHCb with beam-gas imaging, PhD thesis, RWTH Aachen U, 2014, https://inspirehep.net/record/1339684/files/CERN-THESIS-2013-301.pdf.

[43] M. Ferro-Luzzi, Proposal for an absolute luminosity determination in colliding beam experiments using vertex detection of beam–gas interactions, Nucl. Instrum. Methods A553 (2005) 388–399.

[44] LHCb Collaboration, R. Aaij, et al., Precision luminosity measurements at LHCb, J. Instrum. 9 (12) (2014) P12005, arXiv:1410.0149 [hep-ex].

[45] HERMES Collaboration, A. Airapetian, et al., The HERMES polarized hydrogen and deuterium gas target in the HERA electron storage ring, Nucl. Instrum. Methods A540 (2005) 68–101, arXiv:physics/0408137.

[46] C. Barschel, P. Lenisa, A. Nass, E. Steffens, A gas target internal to the LHC for the study of pp single-spin asymmetries and heavy ion collisions, Adv. High Energy Phys. (2015) 463141 (in press).

[47] J.R. Gaunt, W.J. Stirling, Double parton distributions incorporating perturbative QCD evolution and momentum and quark number sum rules, J. High Energy Phys. 03 (2010) 005, arXiv:0910.4347 [hep-ph].

[48] B. Blok, Yu. Dokshitzer, L. Frankfurt, M. Strikman, Perturbative QCD correlations in multi-parton collisions, Eur. Phys. J. C 74 (2014) 2926, arXiv:1306.3763 [hep-ph].

[49] T. Kasemets, M. Diehl, Angular correlations in the double Drell–Yan process, J. High Energy Phys. 01 (2013) 121, arXiv:1210.5434 [hep-ph].

[50] M. Diehl, T. Kasemets, S. Keane, Correlations in double parton distributions: effects of evolution, J. High Energy Phys. 05 (2014) 118, arXiv:1401.1233 [hep-ph].

[51] PHENIX Collaboration, A. Adare, et al., Ground and excited charmonium state production in $p + p$ collisions at $\sqrt{s} = 200$ GeV, Phys. Rev. D 85 (2012) 092004, arXiv:1105.1966 [hep-ex].

[52] CDF Collaboration, D. Acosta, et al., Υ production and polarization in $p\bar{p}$ collisions at $\sqrt{s} = 1.8$-TeV, Phys. Rev. Lett. 88 (2002) 161802.

[53] H.-S. Shao, HELAC-Onia: an automatic matrix element generator for heavy quarkonium physics, Comput. Phys. Commun. 184 (2013) 2562–2570, arXiv:1212.5293 [hep-ph].

[54] H.-S. Shao, HELAC-Onia 2.0: an upgraded matrix-element and event generator for heavy quarkonium physics, arXiv:1507.03435 [hep-ph].

[55] NuSea Collaboration, L.Y. Zhu, et al., Measurement of Υ production for $p+p$ and $p+d$ interactions at 800 GeV/c, Phys. Rev. Lett. 100 (2008) 062301, arXiv:0710.2344 [hep-ex].

[56] ATLAS Collaboration, G. Aad, et al., Measurement of Upsilon production in 7 TeV pp collisions at ATLAS, Phys. Rev. D 87 (5) (2013) 052004, arXiv:1211.7255 [hep-ex].

[57] CMS Collaboration, S. Chatrchyan, et al., Measurement of the $\Upsilon(1S)$, $\Upsilon(2S)$, and $\Upsilon(3S)$ cross sections in pp collisions at $\sqrt{s} = 7$ TeV, Phys. Lett. B 727 (2013) 101–125, arXiv:1303.5900 [hep-ex].

[58] LHCb Collaboration, R. Aaij, et al., Measurement of Upsilon production in pp collisions at $\sqrt{s} = 7$ TeV, Eur. Phys. J. C 72 (2012) 2025, arXiv:1202.6579 [hep-ex].

[59] LHCb Collaboration, R. Aaij, et al., Production of J/ψ and Υ mesons in pp collisions at $\sqrt{s} = 8$ TeV, J. High Energy Phys. 06 (2013) 064, arXiv:1304.6977 [hep-ex].

[60] STAR Collaboration, L. Adamczyk, et al., Suppression of Γ production in d + Au and Au + Au collisions at $\sqrt{s_{NN}} = 200$ GeV, Phys. Lett. B 735 (2014) 127–137, arXiv:1312.3675 [nucl-ex];
STAR Collaboration, L. Adamczyk, et al., Suppression of Γ production in d + Au and Au + Au collisions at $\sqrt{s_{NN}} = 200$ GeV, Phys. Lett. B 743 (2015) 537, Erratum.

[61] A.D. Martin, W.J. Stirling, R.S. Thorne, G. Watt, Parton distributions for the LHC, Eur. Phys. J. C 63 (2009) 189–285, arXiv:0901.0002 [hep-ph].

[62] M.R. Whalley, D. Bourilkov, R.C. Group, The Les Houches accord PDFs (LHAPDF) and LHAGLUE, in: HERA and the LHC: A Workshop on the Implications of HERA for LHC Physics. Proceedings, Part B, 2005, arXiv:hep-ph/0508110.

[63] Particle Data Group Collaboration, K.A. Olive, et al., Review of particle physics, Chin. Phys. C 38 (2014) 090001.
[64] E.J. Eichten, C. Quigg, Quarkonium wave functions at the origin, Phys. Rev. D 52 (1995) 1726–1728, arXiv:hep-ph/9503356.
[65] W. Buchmüller, S.H.H. Tye, Quarkonia and quantum chromodynamics, Phys. Rev. D 24 (1981) 132.
[66] J. Pumplin, D.R. Stump, J. Huston, H.L. Lai, P.M. Nadolsky, W.K. Tung, New generation of parton distributions with uncertainties from global QCD analysis, J. High Energy Phys. 07 (2002) 012, arXiv:hep-ph/0201195.
[67] Y. Feng, J.-P. Lansberg, J.-X. Wang, Energy dependence of direct-quarkonium production in pp collisions from fixed-target to LHC energies: complete one-loop analysis, Eur. Phys. J. C 75 (7) (2015) 313, arXiv:1504.00317 [hep-ph].
[68] G.T. Bodwin, E. Braaten, G.P. Lepage, Rigorous QCD analysis of inclusive annihilation and production of heavy quarkonium, Phys. Rev. D 51 (1995) 1125–1171, arXiv:hep-ph/9407339;
G.T. Bodwin, E. Braaten, G.P. Lepage, Rigorous QCD analysis of inclusive annihilation and production of heavy quarkonium, Phys. Rev. D 55 (1997) 5853, Erratum.
[69] E. Braaten, B.A. Kniehl, J. Lee, Polarization of prompt J/ψ at the Tevatron, Phys. Rev. D 62 (2000) 094005, arXiv:hep-ph/9911436.
[70] M. Kramer, Quarkonium production at high-energy colliders, Prog. Part. Nucl. Phys. 47 (2001) 141–201, arXiv:hep-ph/0106120.
[71] CTEQ Collaboration, H.L. Lai, J. Huston, S. Kuhlmann, J. Morfin, F.I. Olness, J.F. Owens, J. Pumplin, W.K. Tung, Global QCD analysis of parton structure of the nucleon: CTEQ5 parton distributions, Eur. Phys. J. C 12 (2000) 375–392, arXiv:hep-ph/9903282.
[72] R. Sharma, I. Vitev, High transverse momentum quarkonium production and dissociation in heavy ion collisions, Phys. Rev. C 87 (4) (2013) 044905, arXiv:1203.0329 [hep-ph].
[73] H.-S. Shao, H. Han, Y.-Q. Ma, C. Meng, Y.-J. Zhang, K.-T. Chao, Yields and polarizations of prompt J/ψ and $\psi(2S)$ production in hadronic collisions, J. High Energy Phys. 05 (2015) 103, arXiv:1411.3300 [hep-ph].
[74] H. Han, Y.-Q. Ma, C. Meng, H.-S. Shao, Y.-J. Zhang, K.-T. Chao, $\Upsilon(nS)$ and $\chi_b(nP)$ production at hadron colliders in nonrelativistic QCD, arXiv:1410.8537 [hep-ph].
[75] B. Gong, L.-P. Wan, J.-X. Wang, H.-F. Zhang, Polarization for prompt J/ψ and $\psi(2s)$ Production at the Tevatron and LHC, Phys. Rev. Lett. 110 (2013) 042002, arXiv:1205.6682 [hep-ph].
[76] Y. Feng, B. Gong, L.-P. Wan, J.-X. Wang, An updated study for Υ production and polarization at the Tevatron and LHC, arXiv:1503.08439 [hep-ph].